Engineering Science and Technology, an International Journal 24 (2021) 665–670

HOSTED BY

Contents lists available at ScienceDirect

Engineering Science and Technology, an International Journal

journal homepage: www.elsevier.com/locate/jestch

Experimental determination of cooling performance on heat sinks with cone-jet electrospray mode

Abdüssamed Kabakuş [a,*], Kenan Yakut [b], Ahmet Numan Özakın [b], Rıdvan Yakut [c]

[a] Department of Energy Systems Engineering, Artvin Çoruh University, Turkey
[b] Department of Mechanical Engineering, Atatürk University, Turkey
[c] Department of Mechanical Engineering, Kafkas University, Turkey

ARTICLE INFO

Article history:
Received 30 April 2020
Revised 2 November 2020
Accepted 10 November 2020
Available online 30 November 2020

Keywords:
Electrospray cooling
Heat sink
Enhancement ratio
Fin enhancement ratio
Cone-jet mode of ethanol

ABSTRACT

In this study, electrospray cooling characteristics for smooth surface heat sink and finned surface heat sink were investigated. An experimental study was carried out using ethanol for 7 different heat fluxes in the cone-jet mode, in which a stable and continuous droplet diameter is produced. In the experiments, 7 kV voltage, 20 mm nozzle-to-substrate distance, a stainless steel nozzle with 0.61 mm inner diameter (d_i) and 0.45–0.60 ml/min flow rates were used. Due to that the two flow rate values are very close to each other, no difference in the formation of electrospray was observed, but since the amount of fluid sent to the heat sink is higher, at 0.60 ml/min flow rate, 15–44% better a cooling was achieved under different heat fluxes compared to 0.45 ml/min flow rate. In addition, finned heat sink applied for the first time in electrospray cooling provided approximately 1.3–1.6 times better cooling than smooth surface heat sink. The effect of electrospray dripping on cooling in a finned heat sink is expressed by enhancement ratio (ER). Additionally, the change in fin enhancement ratio (FER), which denotes the enhancement of cooling in finned heat sink in comparison to that in finless heat sink, was scrutinized at different surface temperatures. As a result, as a distinction from the studies on improving heat transfer with electrospray cooling, it was suggested that finned surface heat sinks, which were not used before, can be used as an effective parameter to further enhance the heat transfer.

1. Introduction

Thermal management of microelectronics requires high heat flux removal solutions due to the rapid increase in heat flux densities, generated by integrated circuits, per unit area per unit of time [1].

Temperatures at the joints of microelectronics that are exposed to high heat flux increases. This reduces the performances of devices employing joint elements and shortens their life. Different cooling methods are used to keep the temperature of these systems under control at optimum. Impingement air cooling [2], liquid jet cooling [3], microchannel cooling [4], micropump cooling [5] and spray cooling [6] are among the methods used in high heat flux removal. As a result of the previous studies, it is seen that spray cooling has been a very effective method for removing heat in high heat flux systems [7].

Spray cooling is an attractive method compared to many conventional air cooling systems due to its high effectiveness [8]. However, due to the back bounce of sprayed droplets and relatively high power requirement, conventional spray cooling suffers from low cooling efficiency. Additionally, in electrospray, the back bounce of the droplets is prevented by charging them electrically which make them attach to the surface, thereby a more effective cooling than conventional spray is achieved [9]. Electrospray, by using energy efficient liquid atomization of Coulomb forces, provides two-phase cooling, while at the same time providing improved heat transfer with a very small amount of liquid [10].

In addition, in conventional spray cooling technology, limited droplet carrying ability, need for a high-performance mechanical pump for liquid atomization and deficiencies in adjusting droplet size can be counted as other disadvantages of this method [11]. Electrospray is a very useful method to eliminate these disadvantages. Although electrospray atomization occurs as a result of high voltage, the amp level is mili- or even micro-scale. Thus, both the reliability of the system increases and it provides low energy consumption.

* Corresponding author.
E-mail addresses: akabakus@artvin.edu.tr (A. Kabakuş), kyakut@atauni.edu.tr (K. Yakut), ahmet.ozakin@atauni.edu.tr (A.N. Özakın).
Peer review under responsibility of Karabuk University.

https://doi.org/10.1016/j.jestch.2020.11.004
2215-0986/

Other advantages of electrospray are the droplet size is smaller than that obtained by mechanical atomizers, the size distribution of the droplets is usually narrow and the standard deviation is low, production of uniform droplet particles, charged droplets scatter on their own because they repel each other, the movement of charged droplets can be easily controlled by electric fields, ability to change direction or focus, accumulation efficiency of charged droplets on an object is greater than non-charged droplets and easy to apply method [12–15].

In electrospray, high enough voltage is applied while a dielectric fluid is passing through a nozzle, the electrostatic and gravity forces formed at the nozzle tip overcome the surface tension force thus the fluid particles are dispersed from the nozzle tip. This phenomenon is called electrospray. About the electrospray in the literature; studies were carried out in many fields such as mass spectrometry [16], microparticle production [17], surface coating [18], microencapsulation [19], 2D and 3D printing [20], electrospinning [21], microthruster [22,23], combustion systems [24] and drug production [25].

Electrospray is a method of generating a very fine aerosol through electrostatic charging, unlike the more known hydraulic and air spray. As the voltage increased the particle diameters decrease. Thus, total heat transfer area increases. In addition, an increase in the voltage, widens the spray angle and provides a more homogeneous distribution on the heat sink.

It has been observed in the studies that the droplet diameter and spray angle did not change much after the cone jet mode [26] For this reason, the present study was carried out in the cone jet mode.

The working fluid in electrospray studies depends on the surface temperature to be reached, dielectric fluids with low or high boiling points are preferred. In the electrospray cooling system positively charged fluid particles move to the heat sink. Depending on the flow conditions, the fluid particles evaporate, thus the heat is removed from the heated surface. Fig. 1 shows the working principle of the electrospray cooling system.

Considering the studies in the literature, it is focused on nozzle type, nozzle-heat sink distance, electric field intensity, flow rate, fluid, spray mode etc. The main parameters addressed in some studies related to electrospray cooling in the literature are given in Table 1.

Gibbons and Robinson [10] stated that the peak heat transfer coefficient and enhanced radial cooling zone, while having minor dependency on the nozzle diameter in some cases, are mainly dependent on cooling fluid flow rate, and the distance between the nozzle and target surface. They also showed that electrosprays can achieve much higher a heat transfer compared to that in natural convection even at remarkably low flow rates. For 1082 W/m^2 heat flux, 0.108 nozzle inner diameter and 7.5 mm nozzle-substrate distance, the enhancement ratio increases (0–20) as the voltage increases.

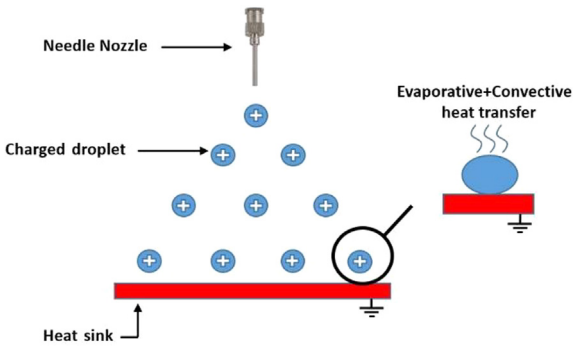

Fig. 1. Schematic representation of the electrospray cooling.

Wang and Mamishev [29] examined the heat transfer performances of Electrospray Evaporative Cooling (ESEC) chambers of different geometries and found out that nozzle geometry affect the heat transfer performance in different ways. At the lowest heat flux, with a 5 mm spacing and 8 nozzles ESEC, a maximum enhancement rate of 1.87 was achieved. By increasing the number and distance between micronozzles, the highest transient cooling rate has been significantly improved. It has been determined that as the flow rate increases and the applied heat flux decreases, the enhancement ratio increases (1–1.8). It was also observed that for 4 nozzles, the enhancement ratio increased (1–1.8) as the distance between the nozzles increased.

Feng and Bryan [30] investigated for the first time the effect of applied electric field on heat transfer achieved by two-phase impingement. They reported that the heat transfer properties of the impinging mass were found to depend on flow rate, applied voltage, distance between nozzle and cooled surface, the nozzle geometry, the heat flux, the geometry of cooled surface, and the nozzle arrangement. It has also been observed that as the voltage increases, the enhancement ratio increases (1–1.5), and as the distance between the substrate-nozzle increases, the enhancement ratio decreases (1.2–1.8).

Chapman et al. [31] have shown that electrospray cooling uniquely capable of enhancing heat/mass transfer for liquid and gas phases, both of which are supported by the electrohydrodynamics of high-momentum electrospray jets.

Jowkar et al. [32] conducted experiments with hemispherical electrospray, conventional electrospray, and drip conditions at same conditions of spray flow rate, and nozzle-to-target surface distance. They observed that the maximum heat flux increased with the increment of the flow rate and voltage, and with the decrement of the distance between the nozzle and tested surface.

Although there are a great many studies in the literature about electrospray, very little has been studied in the field of cooling. Although studies with different flow rates, nozzle diameters, nozzle-to-heat sink distances, and voltages were conducted, electrospray cooling, especially with finned heat sinks, was studied not any too many. No information in available in the literature how the use of fins on the cooling surface affects the heat transfer characteristics in cooling applications by electrospraying. In other words, in electrospray cooling, it is unclear whether the heat that the fluid would draw from the target surface reach higher values with the increase of the temperature or area of the target surface. In this study, the mentioned uncertainty was eliminated and the electrospray cooling characteristics of the smooth surface heat sink and the finned heat sink, which are not yet present in the electrospray cooling literature, were compared. Variations of surface temperature, enhancement ratio, and fin enhancement ratio against the variation of heat flux in finned and non-finned (smooth) surface were examined.

2. Experimental setup

An experimental study was carried out to investigate the electrospray cooling at different flow rates by changing the heat flux on the finned and finless surfaces. For the formation of cone-jet electrospray, which provides stable droplet diameter and speed, fixed 0.61 mm nozzle inner diameter, 20 mm heat sink-nozzle distance, 7 kV voltage and 0.45–0.60 ml/min flow rates were studied. At these flow rates, ethanol completely evaporated. Schematic view of the experimental setup is given in Fig. 2.

In the experiments, pure ethanol, which has high dielectric property, low boiling point, easy evaporation, and low surface

Table 1
An overview table of literature about electrospray cooling.

References	Liquid	Flow Rate	Type of Electrospray	Voltage
Wang et al. [1]	Ethanol	4.2–33.3 μL/min	Multiplexed	4–8 kV
Gibbons and Robinson [8]	Ethanol	2–16 μL/min	Single	2–5 kV
Deng and Gomez [9]	Ethanol + Ionic Liquid	417–1667 μL/min	Multiplexed (Nozzle + extractor)	(V_1-V_2) = 1.5 kV V_2 varied 1–3 kV
Wang and Mamishev [11,27,29]	Ethanol	17–133 μL/min	Single and Multiplexed	4–7.7 kV
Feng and Bryan, [30]	Ethanol	800–9000 μL/min	Single	0–8 kV
Chapman et al. [31]	Methanol	2–8 μL/min	Single	1–4.8 kV
Jowkar et al. [32]	Ethanol	20000–80000 μL/min	Single	7–10 kV
Gibbons and Robinson [33]	Ethanol	2–4 μL/min	Multiplexed	4–8 kV/cm

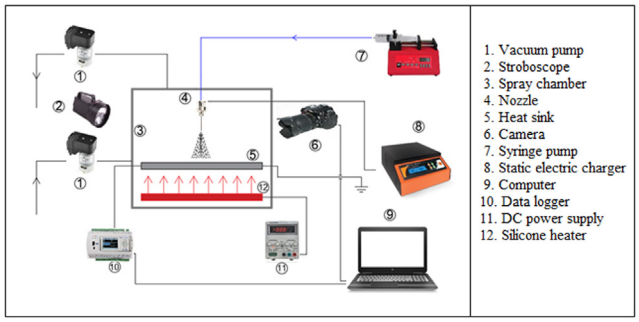

Fig. 2. Schematic view of the experimental setup.

tension, was used. Values for some physical properties of pure Ethanol is given in Table 2.

Ethanol, in different flow rates, was impelled to the stainless nozzle through the syringe pump (New Era, NE-300) with an inside diameter (d_i) of 0.61 mm. A constant voltage of 7 kV is applied to the nozzle by means of a static electric charger (Puls Electronic, HVDC-20). Seven different heat fluxes (7, 7.6, 8.4, 9.1, 9.8, 10.7, 11.4 kW/m^2) were applied with silicone heaters to heat sinks by using a DC power supply (Instek, GPS-3030DD). (see Fig. 3)

Experiments were carried out in the spray chamber in order to ensure constant ambient conditions and to electrically insulate the testing ambience from the outer environment. Through two hoses passing across the back plane of the spray chamber, not affecting the spray flow in the test chamber, air supplement is provided to the test atmosphere by means of a vacuum pump (Airpo D2028B). Furthermore, the air which gets saturated by the evaporated ethanol droplets was expelled through two hoses on the upper surface by means of the vacuum pump. And fresh air was supplied into the chamber. Thus the ambient conditions were kept constant. 36 × 38 × 5 mm smooth aluminum plate and 36 × 38 × 24 mm finned aluminum heat sink, dimensions of which are given in Fig. 4, were used as heat sinks. The side surfaces of the heat sinks were insulated with glass wool so that heat transfer takes place from the upper surface only. The dimensions of the glass wool insulation used are 3.5 × 15 × 15 cm. Within the system, K-type thermocouples, 4 to measure the heat sink temperatures and 1 for ambient temperature, were used. After the system had stabilized and reached steady state conditions, the temperatures measured by thermocouples were transferred to the computer via the data logger (Novus, Fieldlogger).

Table 2
Physical properties of ethanol [34].

Physical Property	Value
Boiling point (°C)	78.3
Density (kg/m3)	790
Surface Tension (N/m)	0.0245
Specific conductivity (pS/m)	130,000

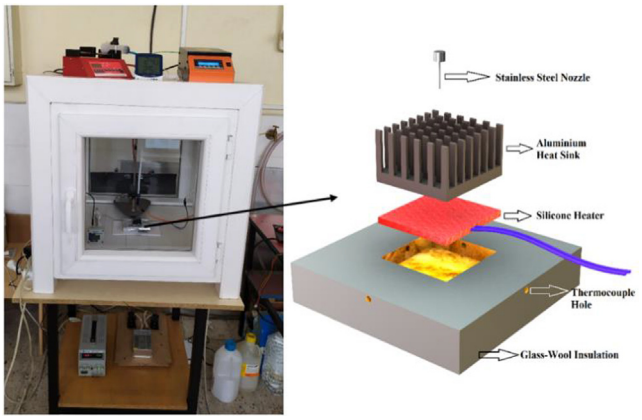

Fig. 3. Experimental setup and Test section.

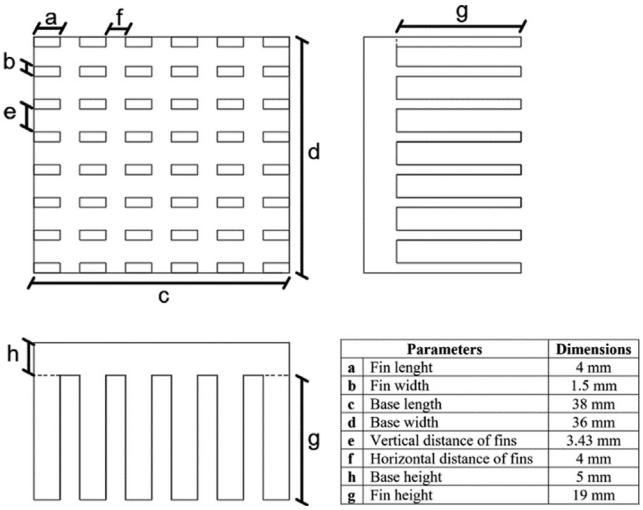

	Parameters	Dimensions
a	Fin lenght	4 mm
b	Fin width	1.5 mm
c	Base length	38 mm
d	Base width	36 mm
e	Vertical distance of fins	3.43 mm
f	Horizontal distance of fins	4 mm
h	Base height	5 mm
g	Fin height	19 mm

Fig. 4. Schematic view and dimensions of the finned heat sink.

For thermocouples and grounding wire, 5 mm deep holes are drilled in the heat sink base. In order for ensuring consistent measurements, the placement of the thermocouples on the heat sink base were done as shown in Fig. 5. Electrospray formation was recorded with Nikon D90 camera using Nikon 18–105 lens. Lutron DT-2199 stroboscope was used as the white light source.

3. Calculations

Total heat transfer from the heat sink surface can be expressed as:

$$\mathbf{Q_{tot} = Q_{con} + Q_{rad} + Q_{vap} + Q_{loss}} \quad (1)$$

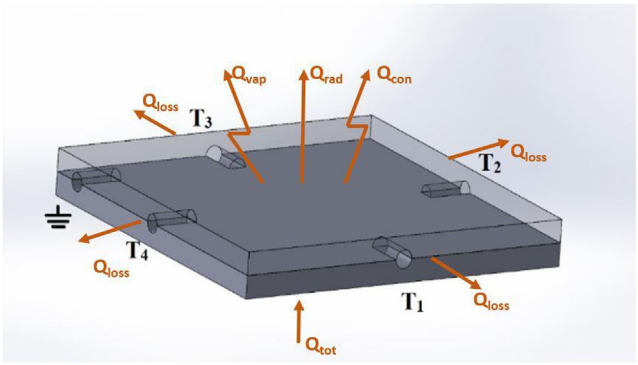

Fig. 5. The placement of thermocouples and the grounding wire in the heat sink base and representation of heat losses from the heat sink.

whereas Q_{tot} is total heat transfer, Q_{con} is convective heat transfer, Q_{rad} is radiative heat transfer, Q_{vap} is evaporative heat transfer, Q_{loss} is the heat loss from the test section. Only the upper surface of the heat sink is open and the vertical side parts are insulated. While convection, evaporation and radiation took place from the upper surface, possible heat loss occurred from the insulated vertical side surfaces. (see Fig. 5) Since the operating temperatures are not too high, heat transfer by radiation, less than 1% of total thermal load, can be neglected. And total heat loss from the test section was calculated as 3% at its maximum. Hence the total amount of heat would be expressed as:

$$\mathbf{Q_{tot} = Q_{con} + Q_{vap}} \tag{2}$$

The convective heat transfer coefficient is calculated using the equation;

$$\mathbf{h = \frac{Q_{tot}}{A_s(T_s - T_\infty)}} \tag{3}$$

whereas h is average heat transfer coefficient, A_s is heat sink surface area, T_s is heat sink average surface temperature, and T_∞ is the ambient temperature in the spray chamber. Q_{tot} being the total heat transferred to heat sink by the silicone heater, V and I the voltage and current applied to the heater, respectively; Q_{tot} can also be expressed as:

$$\mathbf{Q_{tot}} = VI \tag{4}$$

The enhancement ratio (ER) can be expressed as:

$$\mathbf{ER = \frac{h_e}{h_0} = \frac{\Delta T_0}{\Delta T_e}} \tag{5}$$

whereas he is the convective heat transfer coefficient obtained when high voltage is applied to the nozzle, and h_0 is the one obtained when no voltage is applied (dripping mode). ΔT_e and ΔT_0 are, respectively, the difference between the average surface temperature and ambient temperature in the high voltage condition and in no-voltage condition.

The FER figure is used to indicate the effect of finned heat sink on cooling with respect to that of smooth plate. FER is the ratio of the amount of heat drawn from the surfaces of the heat sinks at constant temperature with electrospray, and is defined as:

$$\mathbf{FER = \frac{Q_f}{Q_s}} \tag{6}$$

Q_f is the amount of heat drawn from the finned heat sink, and Q_s, the amount of heat drawn from the smooth plate surface.

Using the uncertainty analysis method by Kline and McClintock [35], experimental uncertainties were calculated to be 4.7% for ER and 0.4% for FER.

$$\mathbf{W_R = \left[\left(\frac{\partial R}{\partial x_1}W_1\right)^2 + \left(\frac{\partial R}{\partial x_2}W_2\right)^2 + \cdots + \left(\frac{\partial R}{\partial x_n}W_n\right)^2\right]^{1/2}} \tag{7}$$

where W_R is the amount of uncertainty consisting of different independent variables (x_1, x_2,..., x_n). R is the function of the independent variables and W_1, W_2,..., W_n are the uncertainty of the independent variables. Experimental uncertainties are as given in Table 3.

4. Results and discussion

The experimental study was aimed at revealing the cooling effects of electrospray on finned and smooth surface at different heat fluxes. Experiments were conducted in cone-jet mode in order to produce droplets with consistent sizes for optimal heat transfer [27,28].

In the experiments carried out at 0.45 and 0.60 ml/min under constant conditions, ethanol completely evaporated. When the amount of fluid that creates the cooling effect is kept constant, with the increase of heat flux, the surface temperature also increased. It is seen that the graphs of finned heat sinks for 0.45 and 0.60 ml/min flow rates are in harmony and their slopes are close. As more fluid comes into contact with the surface at 0.60 ml/min flow rate, obviously more cooling was obtained. In low heat fluxes, the evaporation rate in 0.60 ml/min flow rate has decreased due to that the surface area of the smooth heat sink is limited. Therefore, a higher temperature difference was obtained in 0.60 ml/min compared to 0.45 ml/min.

For 0.45 ml/min flow rate, approximately 34% and 42% better cooling was obtained at minimum heat flux and maximum heat flux, respectively in finned heat sink compared to finless smooth plate. As for 0.60 ml/min flow rate, approximately 29% and 39% better cooling was obtained at minimum heat flux and maximum heat flux, respectively in finned heat sink compared to finless smooth plate. Additionally, in response to the heat flux changes, at 0.6 ml/min flow rate, compared to 0.45 ml/min flow rate, 20–44% and 15–40% better cooling was obtained on the smooth plate's surface and finned heat sink surface, respectively (Figs. 6 and 7).

ER graphs are inversely proportional to ΔT graphs. While ER is high in low heat fluxes, this ratio decreases in high heat fluxes and is almost linear. This is due to the accumulation of ethanol on the heat sink surface in drip mode at low heat fluxes. The accumulation of fluid on the surface causes heat transfer to be inefficient over time. In the cone-jet mode, by the virtue of the fact that the fluid is atomized, it spreads more homogeneously on the plate surface than it does in the drip mode and hence the evaporation rate increases. As the heat flux increases, the evaporation rate and the amount of evaporating fluid also increase in the cone-jet mode, which causes an increase in cooling efficiency. The slope of the graph for 0.45 ml/min flow rate was less due to the fact that the amount of fluid accumulated on the surface at this flow rate was less than that at 0.60 ml/min. It has been observed that while the enhancement ratio for the heat fluxes higher than 9.8 kW/m^2 is between 1.3 and 1.6, it exhibits a sudden rise for heat fluxes lower than 9.8 kW/m^2. In the heat flux range where a complete

Table 3
Accuracy and uncertainty figures of experimental equipment.

Equipment	Accuracy (%)	Uncertainty
Data logger (°C)	±0.2	±1 °C
Syringe pump (ml)	±1	±0.5 ml
Static electric charger (kV)	±0.5	± 0.1 kV
DC Power supply (V)	±0.01	± 5 mV
	±0.2	± 3 mA

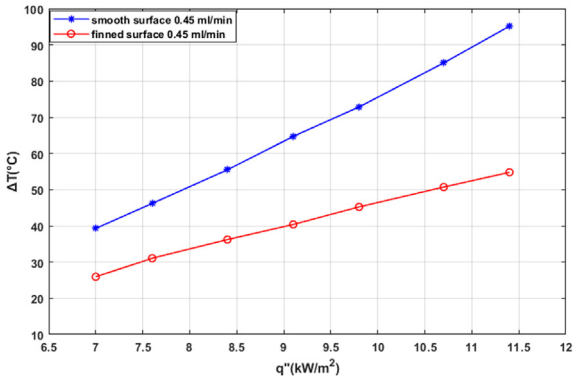

Fig. 6. Variation of temperature difference versus heat flux in smooth plate and finned heat sinks, as a result of electrospray cooling at 0.45 ml/min spray flow rate.

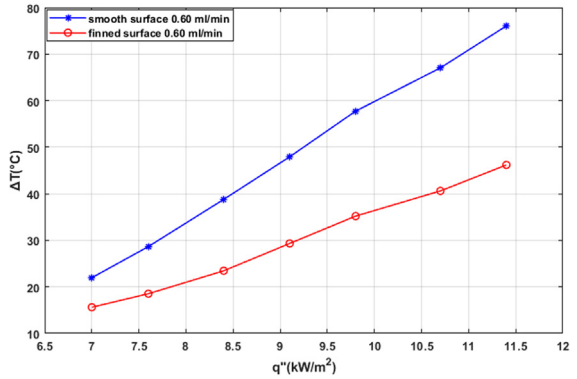

Fig. 7. Variation of temperature difference versus heat flux in smooth plate and finned heat sinks, as a result of electrospray cooling at 0.60 ml/min spray flow rate.

evaporation occurs, the enhancement ratio is approximately 10% better at 0.60 ml/min flow rate than its value at 0.45 ml/min flow rate (Fig. 8).

In order to determine the fin enhancement ratio in heat sinks, the amount of drawn heat was calculated, keeping the heat sink surface temperature constant. At both flow rates, the fin enhancement ratio has also increased since the heat sink surface area increased. While FER was around 1.3 until the boiling point of the fluid, it rose to around 1.55 when the surface temperature rose above the boiling point. As the surface temperature exceeds 78.3 °C, which is the boiling point of ethanol, double-phase cooling took place, where the fluid completely evaporated, and due to the

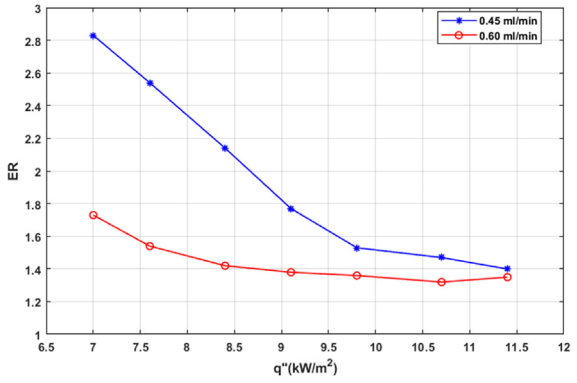

Fig. 8. Enhancement ratio of smooth plate versus heat flux for 0.45 ml/min and 0.60 ml/min flow rates.

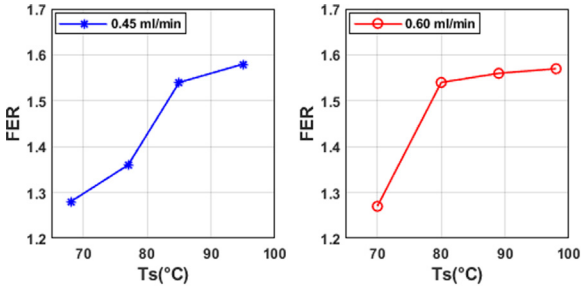

Fig. 9. Fin enhancement ratio of finned heat sink versus surface temperature for 0.45 ml/min and 0.60 ml/min flow rates.

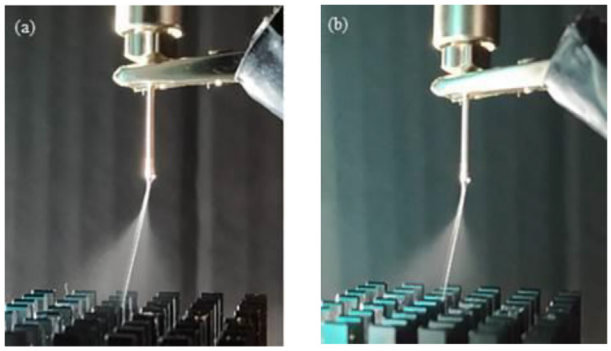

Fig. 10. Electrospray images for 0.45 ml/min (a) and 0.60 ml/min (b) flow rates.

fact that no fluid accumulated on the surface, cooling performance increased. Therefore, FER showed a sudden increase. When the temperature of the plate to be cooled rises above the boiling point of the fluid, the fluid evaporates as soon as it is impinged to the surface, whereby the fin efficiency reaches its maximum value. Beyond the boiling point the FER values, therefore, remain nearly constant. While FER values for 0.45 ml/min and 0.60 ml/min are very close, for the virtue of the fact that the fluid accumulation, which hinders the heat transfer, for temperatures below the boiling point was less, FER value for 0.45 ml/min flow rate was slightly better (Fig. 9).

Because the difference between the two flow rates is very low, the formation of electrospray occurred similarly for both flow rates. However, since more fluid is sent to the heat sink surface at 0.60 ml/min flow rate, more cooling is achieved (Fig. 10).

5. Conclusions

In order to have the system work in cone-jet mode, the experimental study is carried out at values of 7 kV voltage, 20 mm nozzle-to-heat sink distance, 0.61 mm nozzle inner diameter. The performance of electrospray cooling at different heat fluxes and at two different flow rates was investigated. Heat transfer efficiency increased as a result of ethanol evaporated completely and ethanol did not accumulate on the surface for the studied flow rates. Results suggested that, although the electrospray mode did not change for both flow rates, cooling enhancement was better at 0.60 ml/min because more fluid was sent to the heat sink surface. Furthermore, in this study electrospray cooling was performed on finned heat sink for the first time and it was observed that the cooling performance was 1.3–1.6 times better than the flat plate. With this result, it was shown that the surface temperature decreased due to adding fins to the smooth plate and increased the surface area, it also increased the heat transfer through evapora-

tion. In addition to the cases for improving electrospray cooling reported in the literature, heat transfer can further be increased by adding fins to the smooth plate heat sinks, or by simply replacing them. Furthermore, electrospray cooling can be improved by the use of different heat sink geometries or fin optimizations.

Declaration of Competing Interest

The authors declare that they have no known competing financial interests or personal relationships that could have appeared to influence the work reported in this paper.

Acknowledgment

This study was funded by Atatürk University Coordination Unit of Scientific Research Projects under grant no FBA-2018-6965.

References

[1] H. Wang, C.P. Hsu, A.V. Mamishev, The Enhancement ratio of corresponding convection heat transfer coefficent using electrospray evaporative cooling system, in: ASME 2009 Heat Transfer Summer Conference, San Francisco California USA, 2009, https://doi.org/10.1115/HT2009-88629.
[2] R. Yakut, K. Yakut, F. Yeşildal, A. Karabey, Experimental and numerical investigations of impingement air jet for a heat sink, Procedia Eng. 157 (2016) 3–12, https://doi.org/10.1016/j.proeng.2016.08.331.
[3] K. Baghel, A. Sridharan, J.S. Murallidharan, Experimental and numerical study of inclined free surface liquid jet impingement, Int. J. Therm. Sci. 154 (2020), https://doi.org/10.1016/j.ijthermalsci.2020.106389 106389.
[4] D. Deng, Y. Xie, L. Chen, G. Pi, Y. Huang, Experimental investigation on thermal and combustion performance of a combustor with microchannel cooling, Energy 181 (2019) 954–963, https://doi.org/10.1016/j.energy.2019.06.034.
[5] V. Singhal, S. Garimella, Induction electrohydrodynamics micropump for high heat flux cooling, Sens. Actuators A: Phys. 134–2 (2007) 650–659, https://doi.org/10.1016/j.sna.2006.05.007.
[6] F. Yesildal, K. Yakut, Optimization of the spray cooling parameters for a heat sink by the taguchi method, Atomization Sprays 27 (2017) 1063–1075, https://doi.org/10.1615/AtomizSpr.2018019951.
[7] B.S. Glassman, Spray cooling for land, sea, air and space based applications, a fluid management system for multiple nozzle spray cooing and a guide to high heat flux heater design Master of Science Thesis, University of Central Florida, Department of Mechanical, Materials and Aerospace Engineering, Florida, 2005.
[8] M.J. Gibbons, A.J. Robinson, Heat transfer characteristics of single cone-jet electrosprays, Int. J. Heat Mass Transfer 113 (2017) 70–83, https://doi.org/10.1016/j.ijheatmasstransfer.2017.04.119.
[9] W. Deng, A. Gomez, Electrospray cooling for microelectronics, Int. J. Heat Mass Transfer 54 (2011) 2270–2275, https://doi.org/10.1016/j.ijheatmasstransfer.2011.02.038.
[10] M.J. Gibbons, A.J. Robinson, Plume characterisation of a single source electrospray for microelectronic cooling, International Symposium on Electrohydrodynamics, 2014.
[11] H. Wang, A. Mamishev, Design methodology for the micronozzle-based electrospray evaporative cooling devices, J. Electron. Cool. Therm. Control 2 (2012) 17–31, https://doi.org/10.4236/jectc.2012.22002.
[12] U. Badılı, N. Tarımcı, Applications of electrospraying method in nanotechnology, J. Faculty Pharm. Ankara Univ. 38 (2009) 117–135, https://doi.org/10.1501/Eczfak_0000000521.
[13] A. Jaworek, A. Soboczyk, Electrospraying route to nanotechnology: an overview, J. Electrostat. 66 (2008) 197–219, https://doi.org/10.1016/j.elstat.2007.10.001.
[14] A. Jaworek, Micro and nanoparticle production by electrospraying, Powder Technol. 176 (2007) 18–35, https://doi.org/10.1016/j.powtec.2007.01.035.
[15] S. Chakraborty, I.C. Liao, A. Adler, K.W. Leong, Electrohydrodynamics: A facile technique to fabricate drug delivery systems, Adv. Drug Deliv. Rev. 61 (2009) 1046–1054, https://doi.org/10.1016/j.addr.2009.07.013.
[16] J.W. Shi, L.N. Zheng, R.L. Ma, B. Wang, H.Q. Chen, M. Wang, H.F. Wang, W.Y. Feng, Chemical analysis and imaging of fingerprints by air-flow assisted desorption electrospray ionization mass spectrometry, Chin. J. Anal. Chem. 47 (2019) 1909–1914, https://doi.org/10.1016/S1872-2040(19)61205-3.
[17] Y. Hong, Y. Li, Y. Yin, D. Li, G. Zou, Electrohydrodynamic atomization of quasi-monodisperse drug-loaded spherical/wrinkled microparticles, J. Aerosol Sci. 39 (2008) 525–536, https://doi.org/10.1016/j.jaerosci.2008.02.004.
[18] S.A. Barringer, N. Sumonsiri, Electrostatic coating technologies for food proccesing, Annu. Rev. Food Sci. Technol. 6 (2015) 157–169, https://doi.org/10.1146/annurev-food-022814-015526.
[19] A. Jaworek, Electrohydrodynamic microencapsulation technology, Encaptulations 2 (2016) 1–45, https://doi.org/10.1016/B978-0-12-804307-3.00001-6.
[20] B. Zhang, J. He, X. Li, F. Xu, D. Li, Micro/nanoscale Electrohydrodynamic printing: from 2D to 3D, Nanoscale 34 (2016) 1–13, https://doi.org/10.1039/C6NR04106J.
[21] A. Jaworek, A. Sobczyk, A. Krupa, Electrospray application to powder production and surface coating, J. Aerosol Sci. 125 (2018) 57–92, https://doi.org/10.1016/j.jaerosci.2018.04.006.
[22] B.Q. Si, D. Byun, S. Lee, Experimental and theoretical study of a cone-jet for an electrospray microthruster considering the interference effect in an array of nozzles, J. Aerosol Sci. 38 (2007) 924–934, https://doi.org/10.1016/j.jaerosci.2007.07.003.
[23] G. Lenguito, F.J. De La Mora, A. Gomez, Scaling up the power of an electrospray microthruster, J. Micromech. Microeng. 24 (2014) 1–10, https://doi.org/10.1088/0960-1317/24/5/055003.
[24] Z. Jiang, Y. Gan, Y. Ju, J. Liang, Y. Zhou, Experimental study on the electrospray and combustion characteristics of biodiesel-ethanol blends in a meso-scale combustor, Energy 179 (2019) 843–849, https://doi.org/10.1016/j.energy.2019.05.024.
[25] Y. Yang, J. Deng, Z.P. Yao, Field-induced wooden-tip electrospray ionization mass spectrometry for high-throughput analysis of herbal medicines, Anal. Chim. Acta 887 (2015) 127–137, https://doi.org/10.1016/j.aca.2015.06.025.
[26] Z. Wang, L. Xia, L. Tian, J. Wang, S. Zhan, Y. Huo, J. Tu, Natural periodicity of electrohydrodynamic spraying in ethanol, J. Aerosol Sci. 117 (2018) 127–138, https://doi.org/10.1016/j.jaerosci.2017.12.008.
[27] H. Wang, A.V. Mamishev, Heat transfer correlation models for electrospray evaporative cooling chambers of different geometry types, Appl. Therm. Eng. 40 (2012) 91–101, https://doi.org/10.1016/j.applthermaleng.2012.01.061.
[28] A. Jaworek, A. Krupa, Classification of the modes of EHD spraying, J. Aerosol Sci. 30 (1999) 873–893, https://doi.org/10.1016/S0021-8502(98)00787-3.
[29] H. Wang, A.V. Mamishev, Optimization methodology for electrospray evaporative cooling chambers, J. Electrostat. 70 (2012) 384–392, https://doi.org/10.1016/j.elstat.2012.05.003.
[30] X. Feng, J.E. Bryan, Application of electrohydrodynamic atomization to two-phase impingement heat transfer, J. Heat Transfer-Trans. ASME 130 (2008), https://doi.org/10.1115/1.2885178 072202.
[31] J.D. Chapman, P.A. Kottke, A.G. Fedorov, Enhanced thin film evaporation via impinging electrospray liquid jets with entrained air streaming, Int. J. Heat Mass Transfer 131 (2019) 85–95, https://doi.org/10.1016/j.ijheatmasstransfer.2018.11.049.
[32] S. Jowkar, P.M. Jafari, M.R. Morad, Heat transfer characteristics of high flow rate electrospray and droplet cooling, Appl. Therm. Eng. 162 (2019), https://doi.org/10.1016/j.applthermaleng.2019.114239 114239.
[33] M.J. Gibbons, A.J. Robinson, Electrospray array heat transfer, Int. J. Therm. Sci. 129 (2018) 451–461, https://doi.org/10.1016/j.ijthermalsci.2018.03.021.
[34] ISOLAB Laborgeräte GmbH, 2017. Ethanol absolute safety data sheet. <http://www.interlab.com.tr/assets/upload/services/document/920-026-ethanol-absolute64-17-5-en-r-1-pdf23112019075511.pdf> (31.12.2019)
[35] S.J. Kline, F.A. McClintock, Describing uncertainties in single-sample experiments, Mech. Eng. 75 (1953) 3–8.